Leggett-Rice effect in a finite geometry

O. Buu, R. Nyman, R. M. Bowley, and J. R. Owers-Bradley
University of Nottingham, School of Physics and Astronomy, Nottingham NG 7 2 RD, United Kingdom
(Received 1 November 2001; published 20 March 2002)

The problem of restricted diffusion in the presence of the spin rotation effect is investigated theoretically. The concept of diffusion modes is applied to calculate the attenuation of the spin echo signal in a θ-180° NMR sequence. First we study the diffusion modes in a one-dimensional geometry and show that there are in general two types of modes: bulk modes and edge modes. Then we show that the spin rotation effect tends to delocalize the modes and favor edge modes. An expression of the spin echo signal is given as a linear combination of diffusion modes. We study the refocusing of the echo signal and show that the spin rotation effect causes a phase shift. Approximate analytical expressions for the echo signal are given in the three limiting cases: free diffusion, motional narrowing, and localization. Finally, we show that the results of some experiments on spin diffusion anisotropy in spin-polarized ^{3}He$-^4$He mixtures are biased by restricted diffusion effects.

DOI: 10.1103/PhysRevB.65.134512 PACS number(s): 67.65.+z, 76.60.Lz

I. INTRODUCTION

The problem of restricted diffusion in NMR of classical fluids has been investigated thoroughly during the last ten years, and there is a vast literature on this subject (see, for example, Ref. 1). In this paper, we calculate the attenuation of the spin echo signal in a θ-180° NMR sequence in the case of restricted diffusion in quantum systems where the spin rotation effect is present. This applies to degenerate Fermi liquids[2] and also to nondegenerate quantum gases.[3] The study of restricted diffusion in quantum fluids is not only of general interest, but also relevant to NMR experiments on spin diffusion anisotropy in spin-polarized ^{3}He-^{4}He mixtures[4,5] which are currently the subject of controversy.

Leggett[2] derived the equations of motion for the magnetization in a Fermi liquid, but he calculated the echo signal for the case of unbounded diffusion only. Ragan[6] has taken into account boundary effects; however, the perturbative approach that he uses restricts the applicability of his results to the case of fast diffusion. Here, we investigate the spin echo signal in the three limiting cases: free diffusion, motional narrowing, and localization. The analysis follows the approach of Swiet and Sen:[1] we start with a discussion of the diffusion modes in a one-dimensional geometry then, we find an expression for the spin echo signal as a linear combination of diffusion modes. We discuss the three different regimes listed above and conclude with a comment on existing experimental data. The numerical methods used throughout this article are described in the Appendix.

II. FORMULATION

In the following, the z axis is along the applied magnetic field. In a Fermi liquid, the linearized equation of motion for the components of the magnetization perpendicular to the applied magnetic field is[7]

$$\frac{\partial m_-}{\partial t} = i\gamma B(\mathbf{r}) m_- + \frac{D_\perp}{(1+i\mu M_0)} \nabla^2 m_- , \qquad (1)$$

where $m_- = m_x - i m_y$ are the components of the transverse magnetization grouped into a single complex number, $B(\mathbf{r})$ is the z component of the local internal magnetic field in the sample, γ is the gyromagnetic ratio, $D_\perp$ is the transverse diffusion coefficient, M_0 is the longitudinal magnetization, and μM_0 is known as spin rotation parameter. For further reference, we note $D_{\mathrm{eff}} = D_\perp/(1+i\mu M_0)$, the complex effective diffusion coefficient. The conditions of applicability of Eq. (1) are the following: the size of the sample and the characteristic length scale of the magnetic field inhomogeneity must be much larger than the quasiparticle mean free path for Leggett's hydrodynamic equations to be valid; the linear approximation we use throughout this article is valid for $|M_0| \gg |m_-|$, corresponding to a small NMR tipping pulse or nonsaturating continuous-wave NMR. Within this approximation, $|M_0|$ is uniform in the sample and constant in time. Finally, the secular approximation used in Eq. (1) implicitly assumes that the applied magnetic field is very large compared to the local field variations.

In the rest of the article, we investigate the solutions of Eq. (1) in a one-dimensional sample of length $2L$. We assume the walls to be perfectly reflecting for the magnetization, so the boundary condition is $\partial m_-/\partial z = 0$ at $z = \pm L$. We neglect the internal demagnetizing field, an approximation which is valid for ^{3}He-^{4}He mixtures. We only consider the case of a uniform field gradient, so the local field, expressed in the reference frame rotating at the Larmor angular velocity corresponding to the applied magnetic field at the center of coordinates, is simply $B(\mathbf{r}) = Gz$.

For any given initial condition, the magnetization profile $m_-(z,t)$ determined by Eq. (1) can be expressed as a linear combination of eigenmodes:

$$m_-(z,t) = \sum_n c_n \Phi_n(z) e^{\Gamma_n t}, \qquad (2)$$

where Φ_n is the nth eigenmode with complex eigenfrequency Γ_n. The weights of the modes are determined by the initial condition

$$c_n = \int_{-L}^{+L} m_-(z,0)\Phi_n(z)dz. \tag{3}$$

Stoller *et al.*[8] have shown that this expansion breaks down for exceptional values of the coefficient $b = L^3\gamma G/D_{\text{eff}}$. We will ignore this complication and assume that we are always in the case where the Eq. (2) is correct. Thus the whole problem reduces to finding the eigenmodes of Eq. (1) and the corresponding eigenfrequencies. In the following section, we study the diffusion modes in some detail. Although the diffusion modes have been studied by several authors,[7–9] they form the basis for understanding the spin echo signal, which we discuss in Sec. IV.

III. DIFFUSION MODES

The only intrinsic length scale in Eq. (1) is the so-called "dephasing length"[1] $L_c = [|D_{\text{eff}}|/(\gamma G)]^{1/3}$ which is the characteristic distance over which a spin must travel to de-phase by 2π. The ratio L_c/L determines the boundary between the fast diffusion regime ($L_c/L \gg 1$) and the slow diffusion regime ($L_c/L \ll 1$) in classical liquids ($\mu M_0 = 0$). To investigate the eigenmodes with finite μM_0, it is useful to draw on the analogy between Eq. (1) and the Schrödinger equation: the term $-\gamma B(\mathbf{r})$ plays the role of a potential, and the complex coefficient $(i-\mu M_0)/D_\perp$ is the analog of the mass. The imaginary part of the mass analog gives a damping of the modes (i.e., finite real part of the eigenvalues) which physically comes from diffusion processes. In a quantum fluid, the spin rotation effect introduces a restoring force in the dynamics, and the diffusion modes become weakly damped spin-wave modes when $|\mu M_0| \gg 1$. While Eq. (1) is symmetric with respect to $z=0$ when $\mu M_0 = 0$, the molecular field μM_0 breaks this symmetry in a quantum fluid, and the sign of the spin rotation parameter determines whether maximum field-seeking ($\mu M_0 < 0$) or minimum field-seeking ($\mu M_0 > 0$) modes are favored. In the following, we develop these assertions in a more formal way. Our analysis relies on the detailed study of the diffusion modes carried out by Stoller *et al.*[8]

To derive the eigenvalue equation, one looks for a solution of Eq. (1) of the form $m_-(z,t) = \Phi_n(z)e^{\Gamma_n t}$. Multiplying both sides of the equation by $L^3(1+i\mu M_0)/D_\perp$, one obtains the dimensionless equation for the mode Φ_n with the eigenvalue γ_n:

$$\left\{\frac{\partial^2}{\partial\zeta^2} + ib\zeta\right\}\Phi_n = \gamma_n\Phi_n, \tag{4}$$

with the boundary conditions $d\Phi_n/d\zeta = 0$ at $\zeta = \pm 1$. The dimensionless quantities are defined as follows:

$$\zeta = z/L, \quad b = L^3\gamma G/D_{\text{eff}}, \quad \gamma_n = \Gamma_n L^2/D_{\text{eff}}.$$

In the core of the article, we express time in units of $(L|\gamma G|)^{-1}$ and frequency in units of $L|\gamma G|$. For the sake of the discussion, we assume that $\gamma G > 0$. So, in these units, the complex eigenfrequency of the nth mode is $\omega_n = \gamma_n/b$, the real part of ω_n corresponding to the decay rate and the imaginary part to the frequency. As one expects for a stable system, the real part of the eigenfrequency is negative. This can be seen by multiplying each side of Eq. (4) by Φ_n^* and integrating over the length. One obtains

$$\omega_n \int_{\zeta=-1}^{+1} |\Phi_n|^2 d\zeta = i\int_{\zeta=-1}^{+1} \zeta|\Phi_n|^2 d\zeta - \frac{1}{b}\int_{\zeta=-1}^{+1}\left|\frac{d\Phi_n}{d\zeta}\right|^2 d\zeta. \tag{5}$$

The real part of the right-hand side of Eq. (5) is $[-(D/(L^3\gamma G)(1+\mu^2 M_0^2)]\int_{\zeta=-1}^{+1}|d\Phi_n/d\zeta|^2 d\zeta \leqslant 0$. Note that the real part of ω_n vanishes when $|\mu M_0| \to +\infty$ which means that the eigenmodes are undamped in this limit. For further reference, we note $\langle\zeta\rangle_n \equiv \int_{-1}^{+1}|\Phi_n|^2\zeta d\zeta / \int_{-1}^{+1}|\Phi_n|^2 d\zeta$, the average position of the nth eigenmode, which appears in the first term of the right-hand side of Eq. (5).

For $b=0$, Eq. (4) is the diffusion equation. In this case, the modes are

$$\Phi_n(\zeta) = \cos\left(\frac{n\pi}{2}(\zeta+1)\right), \quad \gamma_n = \left(\frac{n\pi}{2}\right)^2. \tag{6}$$

In the fast diffusion limit ($|b|^{-1/3} = L_c/L \gg 1$), the eigenvalue problem can be solved with perturbative methods from the eigenmodes of the $b=0$ case. For further reference, the eigenfrequency of the slowest mode is[8]

$$\omega_0 = -\frac{2}{15}b. \tag{7}$$

To investigate the slow diffusion limit ($L_c/L \ll 1$) we note that Eq. (4) is related to the Airy equation through the substitution $u = (i\zeta - \omega_n)b^{1/3}$, the phase of $b^{1/3}$ being chosen in the sector $[-\pi/3, \pi/3]$. Consequently, the solutions $\Phi_n(\zeta)$ can be formally written as linear combinations of the Airy functions $\text{Ai}(e^{i2\pi/3}u)$ and $\text{Ai}(e^{-i2\pi/3}u)$, the respective amplitudes of the two functions being determined by the boundary conditions. For the relevant modes, as we will see shortly, the wave function $\Phi_n(\zeta)$ can usually be approximated by only one Airy function.

Figure 1 shows a series of plots of eigenvalues in the complex plane calculated with $|b| = 10^4$ and different values of μM_0. The x axis is the real parts of ω_n which corresponds to the damping, and the y axis is the imaginary part which corresponds to the frequency. Let us first comment on the spectrum calculated with $\mu M_0 = 0$ [Fig. 1(a)]. The modes with a real part $\text{Re}(\omega_n) \lesssim -0.5$ do not contribute to the NMR signal since they are strongly damped and their weight c_n is negligible if the initial magnetization is uniform across the cell. We shall not discuss these modes further. The relevant modes [$\text{Re}(\omega_n) \gtrsim -0.5$] lie in the frequency range $1 > \text{Im}(\omega_n) > -1$. There are three branches in the spectrum corresponding to three sorts of modes: upper edge modes, lower edge modes, and bulk modes. The upper edge modes are confined near the upper wall ($\zeta = +1$), so they are not influenced by the lower wall. As a consequence, they can be approximated by solutions of Eq. (4) with the boundary conditions $(d\Phi_n/d\zeta)_{\zeta=+1} = 0$ and $\Phi_n(\zeta) \to 0$ for $\zeta \to -\infty$. Those solutions are

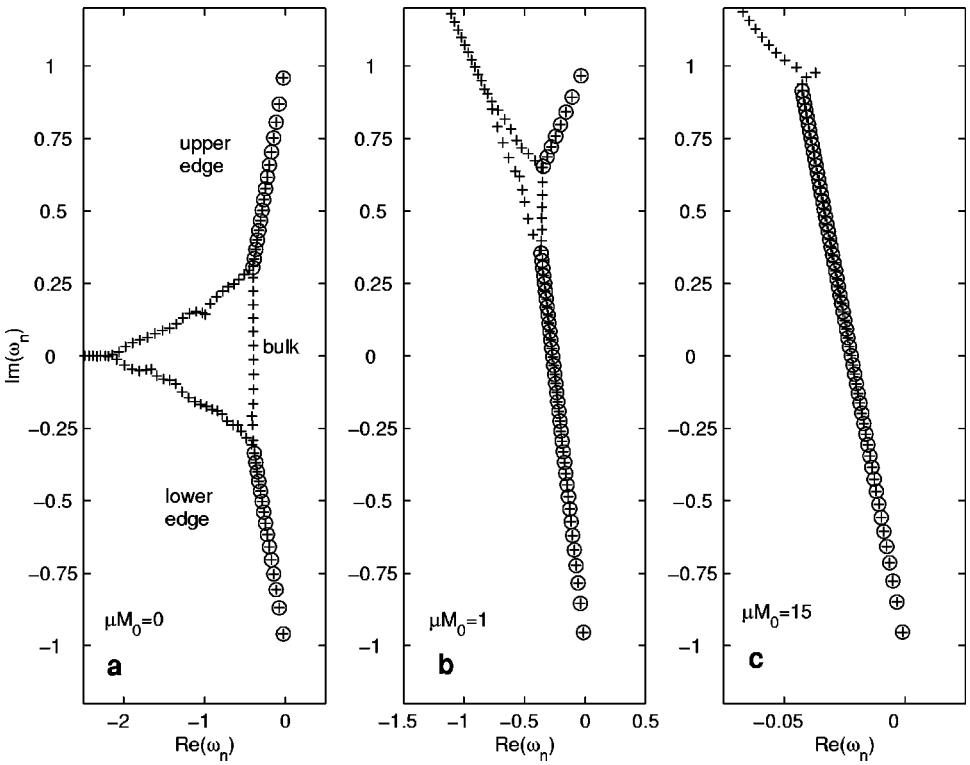

FIG. 1. Plots of the eigenfrequencies ω_n in the complex plane. $\mathrm{Re}(\omega_n)$, on the horizontal axis, is the damping rate of the nth mode. $\mathrm{Im}(\omega_n)$, on the vertical axis, is the frequency. The spectrum of relevant NMR modes can be split into three branches: upper edge modes, lower edge modes, and bulk modes. The crosses are the numerical results, calculated with $|b|=10^4$ and different values of μM_0. The circles correspond to the approximate Eqs. (8b) and (9b).

$$\Phi_n(\zeta)=A_n\mathrm{Ai}(e^{i\pi/6}b^{1/3}(1-\zeta)+\alpha_n), \tag{8a}$$

$$\omega_n=i-\alpha_n b^{-1/3}e^{-i2\pi/3}, \tag{8b}$$

where α_n is the nth zero of the derivative of the Airy function Ai and $A_n^{-1}=b^{-1/6}e^{i7\pi/12}\alpha_n^{1/2}\mathrm{Ai}(\alpha_n)$ is a normalization constant such that $\int_{\zeta=-1}^{+1}\Phi_n^2 d\zeta=1$. Similarly, the lower edge modes are

$$\Phi_n(\zeta)=B_n\mathrm{Ai}(e^{-i\pi/6}b^{1/3}(1+\zeta)+\alpha_n), \tag{9a}$$

$$\omega_n=-i-\alpha_n b^{-1/3}e^{i2\pi/3}, \tag{9b}$$

with $B_n^{-1}=b^{-1/6}e^{i7\pi/12}\alpha_n^{1/2}\mathrm{Ai}(\alpha_n)$.

Bulk modes are localized in the center of the cell, so they are not influenced by either wall. Their eigenfrequencies ω_n can be obtained by perturbation theory[1] from the edge modes in the limit $|b|^{1/3}\gg 1$. For a given complex ω_n, one cannot find solutions of Eq. (4) with the boundary conditions $\Phi_n(\zeta)\to 0$ at $\zeta\to\pm\infty$. However, the functions

$$\Phi_n(\zeta)\propto\mathrm{Ai}(e^{i2\pi/3}u) \quad \text{for } \mathrm{Im}(\omega_n)>0, \tag{10a}$$

$$\Phi_n(\zeta)\propto\mathrm{Ai}(e^{-i2\pi/3}u) \quad \text{for } \mathrm{Im}(\omega_n)<0 \tag{10b}$$

are solutions of Eq. (4) and take small values for $\zeta\to\pm 1$. They are found to be very good approximations to the exact numerical solutions.

The spectrum in the case of $\mu M_0=0$ is symmetric with respect to the real axis, reflecting the symmetry of the Eq. (4) with respect to $\zeta=0$. On increasing $|\mu M_0|$, one sets a preferred direction in the problem, and one sort of edge modes is favored. Lower edge modes are favored if the phase of b is in the first or third quadrant in the complex plane $(\mathrm{Arg}(b)\in]0,\pi/2[\cup]\pi,3\pi/2[)$; upper edge modes are favored in the remaining cases. At the same time, the amplitudes of the real parts of the eigenfrequencies decrease; i.e., the modes become more weakly damped [see Fig. 1(b)]. Eventually, for large values of $|\mu M_0|$, the spectrum is entirely made up of edge modes of one sort [Fig. 1(c)]. For $|\mu M_0|=+\infty$, the eigenfrequencies are purely imaginary, which corresponds to undamped modes.

It is useful to visualize the eigenfunctions to understand the difference between the "classical modes" ($\mu M_0\approx 0$) and the "quantum modes" ($|\mu M_0|\gg 1$). In the case of classical diffusion [Fig. 2(a)], the modes are localized about the position corresponding to their eigenfrequency $\langle\zeta\rangle_n=\mathrm{Im}(\omega_n)$. In the limit of a strong spin rotation effect, the diffusion problem is analogous to a Hermitian quantum mechanical problem. Hence, the modes are similar to delocalized quantum mechanical wave functions [Fig. 2(b)]. In the case of minimum seeking modes, for example, the wave functions change from oscillatory in the region between the lower wall and the confining potential $[-1<\zeta<\mathrm{Im}(\omega_n)]$ to exponentially decaying above $[\mathrm{Im}(\omega_n)<\zeta<1]$. As usual, there is a turning point at the crossover with the potential $[(d^2\Phi_n/d\zeta^2)_{\zeta=\mathrm{Im}(\omega_n)}=0]$.

To understand how this difference in behavior arises from the same functional expressions [Eqs. (8), (9), and (10)], we consider the contour map of the real part of the function $\mathrm{Ai}(X+iY)$ in the complex plane (X,Y). As ζ varies from -1 to $+1$, the trajectory of the variable $v(\zeta)=e^{-i2\pi/3}(i\zeta-\omega_n)b^{1/3}$ in the complex plane is a finite straight line. To make the connection with the wave functions, the real part of $\Phi_n(\zeta)$ would correspond to a plot of the altitude as a function of ζ along the trajectory $v(\zeta)$. Let us first consider an eigenmode in the case $\mu M_0=+\infty$. This mode is a lower edge mode of the form [Eq. (9)], so the line $v(\zeta)$ lies on the

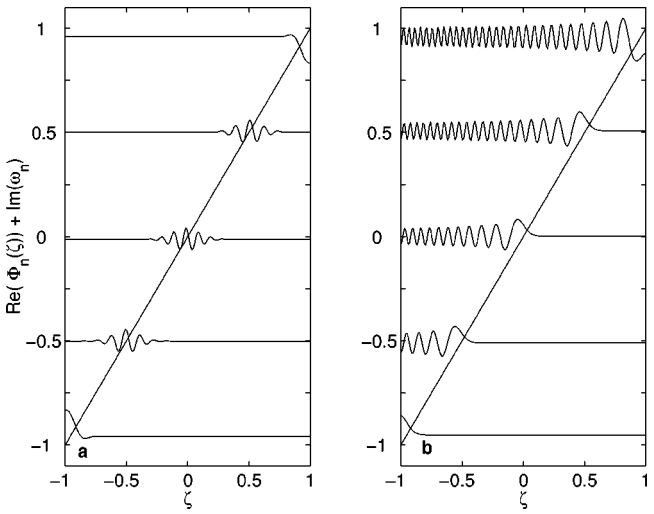

FIG. 2. Real part of selected eigenfunctions $\Phi_n(\zeta)$ calculated with $\mu M_0=0$ (a) and $\mu M_0=+\infty$ (b). The wave functions have been offset by the imaginary part of their eigenfrequency. The two figures clearly display the difference between the localized classical diffusion modes and the delocalized spin-wave modes.

real axis, one end of the line being at the coordinate $(\alpha_n,0)$. As can be seen in Fig. 3(a), the line intercepts a region of rugged landscape for $\alpha_n<X<0$ and falls off as $\sim X^{-1/4}e^{-2X^{3/2}/3}$ in the region $X>0$.[10] The corresponding altitude plot is one of the wavefunctions shown in Fig. 2(b). Let us now turn to the case $\mu M_0=0$ and consider a bulk mode of the form expressed by Eq. (10b). Now, the line $v(\zeta)$ lies off the real axis. As shown in the Fig. 3(b), the line crosses a region where the Airy function is oscillatory for $\zeta \approx \mathrm{Im}(\omega_n)$, and extends to regions where the ''landscape'' is flat for $\zeta\rightarrow\pm 1$.

IV. SPIN ECHO

The technique of ''spin echoes'' is a standard NMR sequence which consists of letting the magnetization evolve for a time t_e after a first excitation pulse and applying a second pulse to rotate the magnetization through 180°. During the first evolution period, the signal decays due to the dephasing of the magnetization in different parts of the sample caused by the field gradient and diffusion. After the reversing 180° pulse, the magnetization rephases, so an ''echo'' signal is observed at time $\simeq 2t_e$. The amplitude of the echo signal depends on two intrinsic length scales: the dephasing length L_c and the diffusion length $L_d=(|D_{\mathrm{eff}}|t_e)^{1/2}$. There are now three different regimes to consider, depending on which of the length scales—L_d, L_c, or L—is the shortest: free diffusion ($L_d \ll L_c, L$), motional narrowing ($L \ll L_d, L_c$), and localization ($L_c \ll L_d, L$). In the linear approximation, the consequence of the spin rotation effect on the echo amplitude is simply to renormalize the spin diffusion coefficient $D_\perp \rightarrow D_{\mathrm{eff}}$. The main difference with the classical case is that the echo signal refocuses with a different phase. This effect occurs because the refocusing takes place under a reversed molecular field $-\mu M_0$, so the isochromats[11] do not rotate at the same velocity after and before the 180° pulse. In this section, we give an expression for the echo signal as a function of the diffusion modes. From this expression, we discuss the three different regimes, giving in each case an approximate form for the echo amplitude and phase.

A. Formal expression for the spin echo signal

For the sake of simplicity, we assume the transverse excitation field to be uniform and directed along the y axis. Without loss of generality, we take that $\mu M_0>0$ at time $\tau=0$. The magnetization during the evolution period following the first excitation pulse is still given by Eq. (2). The free induction decay (FID) signal is given by

$$S(\tau)=\int_{-1}^{+1} m_-(\zeta,\tau)d\zeta=\sum_n c_n^2 e^{\omega_n\tau} \quad (\tau<\tau_e). \quad (11)$$

The weights are given by $c_n=\int_{-1}^{+1}\Phi_n(\zeta)d\zeta$. The 180° pulse at time τ_e causes the transformation $M_0\rightarrow -M_0$; $m_-(\zeta,\tau_e^-)\rightarrow -m_-^*(\zeta,\tau_e^+)$, where the symbol * denotes the complex conjugate. The magnetization evolution after the 180° pulse can be described by an expression analogous to Eq. (2). However, due to the reversal of longitudinal magnetization, the relevant eigenmodes Φ_m' with eigenfrequencies ω_m' are now maximum field seeking, and their amplitudes are determined by the nonuniform magnetization profile $m_-^*(\zeta,\tau_e^+)$. The expression for the echo signal is

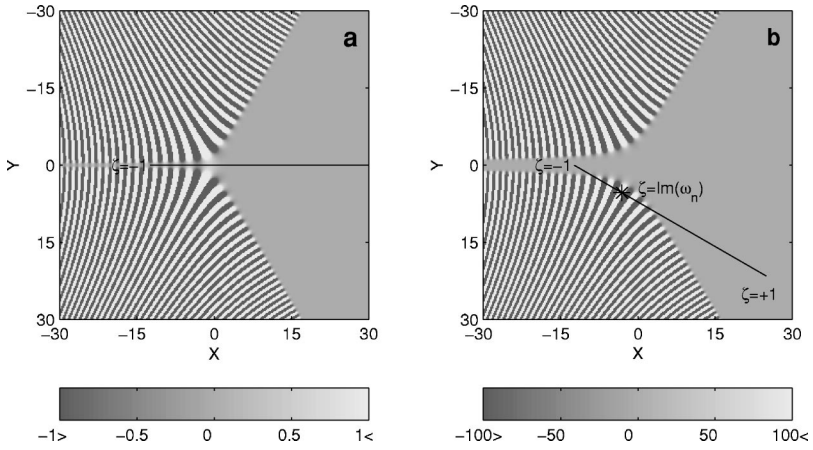

FIG. 3. Gray scale maps of the real part of the Airy function in the complex plane seen with two different vertical scales. The straight line represents the trajectory of the variable $v(\zeta)$ in the complex plane. (a) For an edge mode in the limit $\mu M_0=+\infty$, the line intercepts a region of rugged ''landscape'' for $\alpha_n<X<0$ and falls off as $\sim X^{-1/4}e^{-2X^{3/2}/3}$ in the region $X>0$. (b) For a bulk mode calculated with $\mu M_0=0$, the line extremities lie in flat regions where $\mathrm{Ai}(X+iY)$ takes small values. The star indicates the point where $\zeta=\mathrm{Im}(\omega_n)$.

$$S(\tau) = -\sum_{n,m} e^{\omega_n^* \tau_e} c_n^* U_{mn} c'_m e^{\omega'_m(\tau-\tau_e)} \quad (\tau > \tau_e), \quad (12)$$

where the matrix $U_{nm} = \int_{-1}^{+1} \Phi_n^*(\zeta)\Phi'_m(\zeta)d\zeta$ is the overlap between the maximum field-seeking modes and the minimum field-seeking modes.

We now use Eq. (12) to discuss the echo formation. Due to the symmetry of the linear field profile with respect to $\zeta = 0$, the maximum field-seeking and the minimum field-seeking modes are related through $\omega'_m = \omega_m^*$ and $\Phi'_m(\zeta) \propto \Phi_m^*(-\zeta)$. Consequently, the factors $e^{\omega_n^* \tau_e} c_n^* U_{mn} c'_m e^{\omega'_m \tau_e}$ are symmetric under the interchange of m and n, so we can rewrite the terms in the sum as $O_{mn} e^{i\Delta_{mn}} e^{\omega'_m \delta\tau}$, where O_{mn} and Δ_{mn} are two real symmetric matrices. Using the symmetry properties of O_{mn} and Δ_{mn}, and noting $\delta\tau = \tau - 2\tau_e$, we can express the amplitude of the echo signal as

$$|S(\tau)|^2 = \sum_{n,m,m',n'} O_{mn} O_{m'n'} \cos[\Delta_{mn} - \Delta_{m'n'} + i(\omega_m - \omega_{m'} + \omega_n - \omega_{n'})\delta\tau/2] \times \cos[i(\omega_m - \omega_{m'} - \omega_n + \omega_{n'})\delta\tau/2]. \quad (13)$$

In Eq. (13), the factors $\cos[i(\omega_m - \omega_{m'} - \omega_n + \omega_{n'})\delta\tau/2]$ ensure that all the terms in the sum come back into phase at $\tau = 2\tau_e$. This refocusing gives rise to the echo signal $S(2\tau_e)$ whose amplitude h and phase ϕ are usually measured in experiments. Note that in the presence of higher-order terms in the field profile, which break the symmetry with respect to $\zeta = 0$, the refocusing takes place at $\tau \neq 2\tau_e$. In particular, numerical studies show that in the presence of a quadratic field term $\frac{1}{2}G_2(2z^2 - x^2 - y^2)$ with a cylindrical geometry, the echo is delayed for $\mu M_0 G_2 L/G > 0$ and advanced for $\mu M_0 G_2 L/G < 0$.

In classical NMR ($\mu M_0 = 0$), the diffusion modes are localized. As a consequence, the overlap matrix is quasidiagonal, so the only terms in Eq. (12) contributing to the echo signal are of the form $|c_n|^2 e^{2\mathrm{Re}(\omega_n)\delta\tau}$. Hence, the "classical" echo will refocus with $\phi = \pi$. The situation is different in the presence of the spin rotation effect. As the diffusion modes are delocalized, the overlap matrix is no longer diagonal, and the echo signal will generally refocus with a phase shift for finite μM_0. There is also a difference in the echo attenuation mechanism between the classical case and the pure quantum case. In the classical case, the Hahn echo completely refocuses the decoherence due to inhomogeneous broadening, and the echo attenuation is due to diffusion only. Indeed, in this case, there are no crossed terms in Eq. (12) since the overlap matrix is diagonal, and the echo decay depends only on the real part of the eigenfrequencies. In the pure quantum case ($|\mu M_0| \to +\infty$), by contrast, the diffusion modes are undamped; i.e., their eigenfrequencies are purely imaginary. Therefore, the signal decay during the evolution period is reversible. Nonetheless, the magnetization is not totally refocused at the echo because the evolution after the 180° pulse takes place under a reversed molecular field.

Equation (12) is an exact formula which allows us to calculate the spin echo signal numerically. We can obtain approximate analytical expressions in the limiting cases described at the beginning of this section. We now proceed with the study of these limiting regimes.

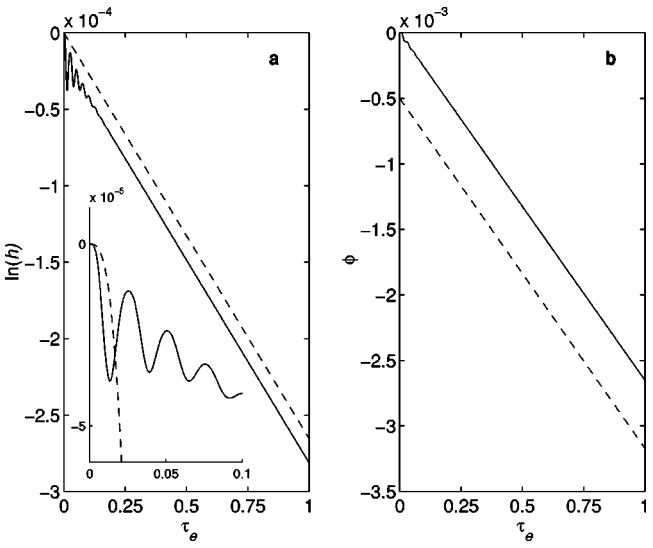

FIG. 4. Echo signal calculated for $|b| = 0.01$ and $\mu M_0 = 10$. The solid lines are the exact numerical results. (a) Amplitude of the echo as a function of the waiting time. For long waiting time, the decay of the echo is well described by the approximate expression (16), valid in the motional narrowing regime (dashed line). For the very short waiting times, the echo amplitude decays according to Eq. (14) for free diffusion (dashed line in the insert). (b) Phase of the echo as a function of the waiting time. The dashed line corresponds to the approximate formula (17). The dashed line has been offset by -0.5 rad for clarity.

B. Free diffusion

When $L_d \ll L_c, L$, the diffusion occurs on a time scale too short for the spins to "see" the walls. The attenuation factor of the echo signal is given by the Leggett's expression for unbounded diffusion:[2]

$$h = \exp\left(-\frac{2}{3}\frac{\tau_e^3}{|b|\sqrt{1+\mu^2 M_0^2}}\right) = \exp\left(-\frac{2}{3}\frac{(\gamma G)^2 D_\perp}{1+\mu^2 M_0^2} t_e^3\right). \quad (14)$$

As one expects, the decay rate does not depend on the size of the sample in this limit. If $\mu M_0 = 0$, one finds the familiar expression for the echo attenuation of the Hahn echo in classical liquids.[11] In quantum liquids, the phase of the echo depends implicitly on the waiting time according to the relation:

$$\phi = -\mu M_0 \ln(h). \quad (15)$$

In practice, free diffusion is observed for a short waiting time τ_e for any value of the parameter b. However, the time scale over which the regime of free diffusion is observed can be very short if $|b|$ is small [see insets in Figs. 4(a) and 5(a)].

C. Motional narrowing

In the limit $L \ll L_c, L_d$, the spins diffuse rapidly across the cell, so the magnetization remains essentially uniform. In the presence of the spin rotation effect, the magnetization is rotated off the (x,z) plane by an angle proportional to $\mu M_0 t_e$. In the language of diffusion modes, this so-called ''motional narrowing regime'' corresponds to the limit of $|b|^{1/3} \ll 1$ and long waiting time ($\tau_e \gg |b|$). The only long-lived mode is the lowest eigenmode, which for small $|b|$ is nearly uniform across the cell, with a complex eigenfrequency given by Eq. (7). Accordingly, the magnetization profile during the evolution period can be written as $m_-(\zeta,\tau) \simeq e^{-2b\tau/15}$. The 180° pulse transforms the magnetization $m_-(\zeta,\tau_e)$ into $m_-^*(\zeta,\tau_e)$, whence the eigenmode evolves with the complex frequency $-\frac{2}{15}b^*$. Consequently, the echo signal attenuation is twice the signal attenuation during the evolution period:

$$h \propto \exp\left(-\frac{4}{15}\mathrm{Re}(b)\tau_e\right) = \exp\left(-\frac{4}{15}\frac{L^4(\gamma G)^2}{D_\perp}t_e\right). \quad (16)$$

It is remarkable that the echo signal decays according to the classical rate,[12] independent of μM_0. This result was obtained by Ragan.[6] The difference between $\mu M_0 = 0$ and finite μM_0 is in the phase shift of the echo signal, which is twice the phase built up from $\tau = 0$ to $\tau = \tau_e$:

$$\phi = \frac{4}{15}\mathrm{Im}(b)\tau_e = \frac{4}{15}\frac{L^4(\gamma G)^2}{D_\perp}\mu M_0 t_e. \quad (17)$$

Figure 4 shows the amplitude and phase of the echo signal as a function of the waiting time τ_e calculated with $|b| = 0.01$ and $\mu M_0 = 10$. For short τ_e, the signal attenuation follows Eq. (14). For longer τ_e, one enters the motional narrowing regime, and the phase and attenuation of the echo signal are given by formulas (16) and (17).

D. Localization

The third limiting case $L_c \ll L, L_d$ has been called the localization regime.[1] It corresponds to the regime of long waiting time ($\tau_e \gg |b|^{1/3}$) for $|b|^{1/3} \gg 1$. Again, in this case, the signal originates mainly from the lowest eigenmode. However, for strong b, the lowest eigenmode is an edge mode, which is localized near a wall. By the same argument as for the case of motional narrowing, and using Eqs. (9b) and (8b) for the edge modes eigenfrequency, we obtain

$$h \propto \exp\{-\alpha_0 |b|^{-1/3}[\cos(\varphi/3) - \sqrt{3}|\sin(\varphi/3)|]\tau_e\}$$
$$= \exp\left(-\alpha_0 \frac{(\gamma G)^{2/3} D_\perp^{1/3}}{(1+\mu^2 M_0^2)^{1/6}} \times [\cos(\varphi/3) - \sqrt{3}|\sin(\varphi/3)|]t_e\right), \quad (18)$$

where $\alpha_0 \approx -1.0188$ and the parameter φ is determined by $\cos(\varphi) = (1+\mu^2 M_0^2)^{-1/2}$ and $\sin(\varphi) = \mu M_0 (1+\mu^2 M_0^2)^{-1/2}$. The phase shift, ignoring a constant term, is obtained similarly:

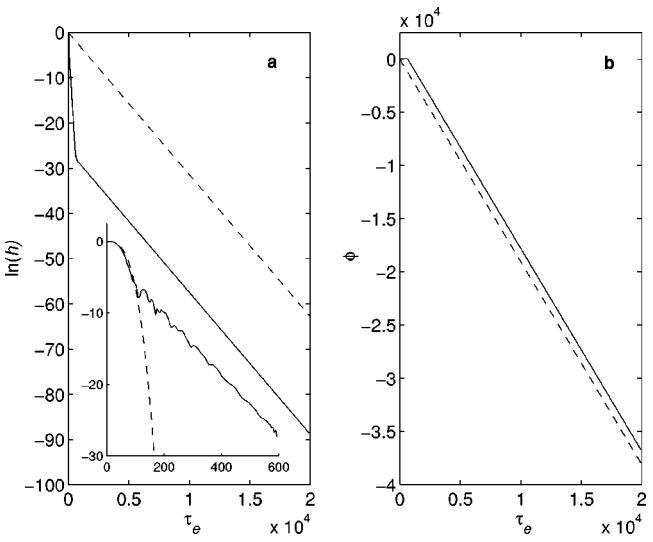

FIG. 5. Echo signal calculated for $|b| = 10^4$ and $\mu M_0 = 10$. The solid lines are the exact numerical results. (a) Amplitude of the echo as a function of the waiting time. For long waiting time, the decay of the echo is well described by Eq. (18) valid in the localization regime (dashed line). Note that in this regime, the signal amplitude is very small. For the very short waiting times, the echo amplitude decays according to Eq. (14) for free diffusion (dashed line in the insert). (b) Phase of the echo as a function of the waiting time. The dashed line corresponds to the approximate formula (19).

$$\phi = \{2\epsilon - \alpha_0 |b|^{-1/3}[\epsilon\sqrt{3}\cos(\varphi/3) - \sin(\varphi/3)]\}\tau_e$$
$$= \left(2\gamma G L \epsilon - \alpha_0 \frac{(\gamma G)^{2/3} D_\perp^{1/3}}{(1+\mu^2 M_0^2)^{1/6}} \times [\epsilon\sqrt{3}\cos(\varphi/3) - \sin(\varphi/3)]\right) t_e, \quad (19)$$

where $\epsilon = +1$ if $\mu M_0 > 0$, $\epsilon = -1$ if $\mu M_0 < 0$, and $\epsilon = 0$ if $\mu M_0 = 0$. For $\mu M_0 = 0$, there is no phase shift, and the decay rate $-\alpha_0 (\gamma G)^{2/3} (D_\perp)^{1/3}$ corresponds to the classical case treated by Swiet and Sen.[1]

Figure 5 shows that, for long waiting times τ_e, the phase and amplitude of the echo signal are well described by Eqs. (18) and (19). However, as Swiet and Sen[1] pointed out, there is little hope of observing the pure localization regime experimentally, since it corresponds to long waiting times and therefore to a vanishingly small NMR signal.

V. COMMENT ON EXISTING NMR DATA

During the last ten years, there has been a controversy about the temperature dependence of the transverse magnetization relaxation time in degenerate Fermi liquids: Meyerovich and Musaelian[13] predicted that this relaxation time should saturate at low temperature as $\propto 1/(T_a^2 + T^2)$, where T_a is the so-called anisotropy temperature. Fomin,[14] on the contrary, calculated that the transverse relaxation time obeys the usual $1/T^2$ dependence. As both the diffusion coefficient and the spin rotation parameter are proportional to this transverse relaxation time, much of the experimental effort has

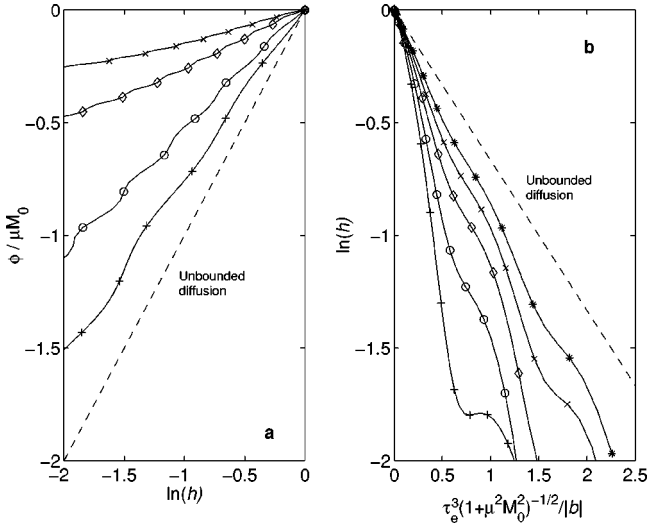

FIG. 6. (a) The echo phase ϕ normalized by the spin rotation parameter as a function of ln(h) calculated with $|b_L|=10^4$ and $\mu M_0=10$ (+), $\mu M_0=30$ (○), $\mu M_0=100$ (◇), and $\mu M_0=200$(×). The dashed line of slope 1 is the case of the unbounded diffusion. In graph (a), the slope gives an "apparent value" of μM_0 which saturates as the spin rotation parameter μM_0 becomes large. (b) Echo heights, ln(h) as a function of $\tau_e^3|b|^{-1}(1+\mu^2M_0^2)^{-1/2}$ calculated with $\mu M_0=10$ and $|b_L|=10^2$ (+), $|b_L|=3\times10^2$ (○), $|b_L|=10^3$ (◇), $|b_L|=3\times10^3$ (×), and $|b_L|=10^4$ (*). The dashed line of slope 2/3 represents the case of unbounded diffusion.

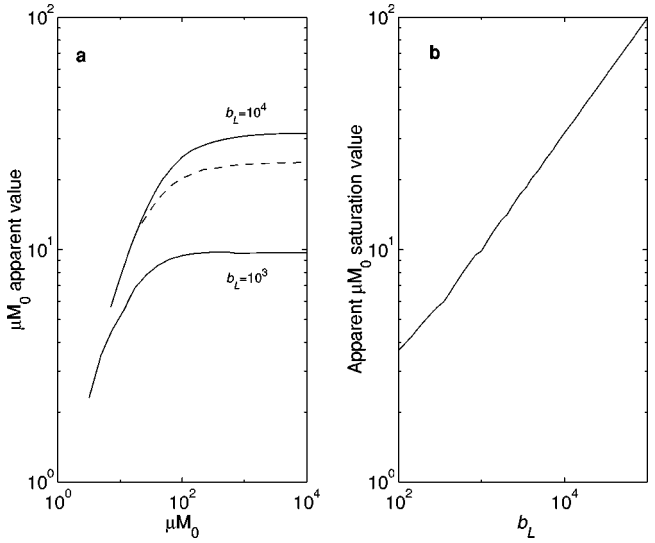

FIG. 7. (a) Slope of the relation ϕ vs ln(h) as a function of μM_0 for $|b_L|=10^3$ and 10^4. The dotted line is a calculation for a right cylinder with a quadratic field term of strength $G_2L/G=0.2$. (b) Saturation value of the "apparent" μM_0 as a function of the parameter b_L. The saturation value is approximately $\propto b_L^{1/2}$.

been concentrated on measuring $D_\perp$ and μM_0 as a function of the temperature. Unfortunately, the experiments so far have given contradictory results.[4,5,15,16] As we shall show, restricted diffusion effects may explain some of the discrepancies between the experimental results.

Hitherto, the experiments employing the method of spin echo have been analyzed assuming that the walls of the experimental cell had no effect on the echo signal. Consequently, the parameter μM_0 for each temperature was determined by linear fitting of the echo phase as a function of the echo amplitude, according to Eq. (15) valid in the regime of free diffusion. Similarly, $D_\perp$ was determined by fitting the echo amplitude as a function of $-\frac{2}{3}(\gamma G)^2 t_e^3/(1+\mu^2M_0^2)$ [Eq. (14)]. In most of the experiments, the value of the parameter L/L_c is in the range 10–100. For these values of L/L_c, the deviation from the free diffusion regime is significant at long time t_e. As we shall see, this deviation has important implications with regard to the analysis of experimental data.

In order to compare experiments to the numerical results, it is convenient to define the temperature-independent parameter $b_L=L^3\gamma G\mu M_0/D_\perp$. During an experiment the field gradient is usually kept at a fixed value; thus b_L is a constant while the parameter $|\mu M_0|$ increases (and possibly saturates) with decreasing temperature. In Fig. 6(a), we show the relation between the phase ϕ normalized by μM_0 and ln(h) plots computed numerically for $b_L=10^4$ for different values of μM_0. In the absence of restricted diffusion effects, the relation $\phi/\mu M_0$ versus ln(h) should be linear with a slope of 1 [Eq. (15)]. For finite b_L, this relation is no longer linear. The deviations from the linear behavior, however, are not large and can be mistaken for the scatter of the data points. More significantly, the average slope of ϕ versus ln(h) is smaller than expected in the case of unbounded diffusion. This deviation from Leggett's prediction leads to an underestimate of μM_0 at low temperature. A similar effect can be seen in Fig. 6(b) for ln(h) versus $[1+(\mu M_0)^2]^{-1/2}|b|^{-1}\tau_e^3$. Consequently, restricted-diffusion effects bias the apparent parameters $D_\perp$ and μM_0 in such a way as to mimic the saturation of the transverse relaxation time at low temperature. Note that the deviations from the free diffusion regime become more severe for decreasing $|b_L|$ and increasing μM_0, since the system gets closer to the localization regime.

In order to illustrate this point, we have compared the values of μM_0 that were used as inputs to the simulation and the value obtained from a linear fit of the simulated ϕ versus ln(h) in the range $-2<\ln(h)<0$. As can be seen in Fig. 7(a), the fitted value deviates from the actual μM_0 and eventually saturates for large μM_0. Numerically, the apparent μM_0 saturation value was found to depend on the parameter b_L as $\propto b_L^{1/2}$ [Fig. 7(b)]. We have also calculated a more realistic case, taking into account the effect of a second-order field gradient in a cylindrical geometry. As shown in Fig. 7(a), for a small second-order gradient, the saturation value of the apparent parameter μM_0 is altered, but the qualitative behavior remains the same.

In the latest experiment in our group,[5] the values for the dimensionless parameters were $b_L\simeq10^4$ with a second-order gradient $G_2L/G\simeq0.2$, leading to an apparent saturation of μM_0 at a value of -27.5. In terms of anisotropy temperature, such a saturation value of the spin rotation parameter would correspond to an apparent T_a of 9 mK for 6.4% ^{3}He-^{4}He mixture at 11.3 T, based on the spin rotation parameter data of Ishimoto *et al.*[17] Consequently, we infer that the value of $T_a=13$ mK reported in our earlier publication[5]

is largely due to finite-size effects. By contrast, for the experiment of Wei *et al.*,[16] the value of parameter b_L was 7.4×10^4, so we expect the effect of restricted diffusion to be relatively small. Using the data of Candela *et al.*,[7] the corresponding apparent anisotropy temperature would be 3 mK in pure ^{3}He at 8 T, which is much smaller than the value of 16 mK reported in Ref. 16.

VI. CONCLUSIONS

We have studied the problem of restricted diffusion in the presence of the spin rotation effect. In a one-dimensional geometry, the diffusion modes fall into two categories: bulk modes, which are not influenced by the presence of the walls, and edge modes, which are confined against a wall. We have shown that the spin rotation effect favors one sort of edge modes, the confinement position of which depends on the sign of the parameter μM_0. Moreover, the diffusion modes are localized for $\mu M_0=0$ and become delocalized when $|\mu M_0|$ is large—that is, when the restoring force provided by the spin rotation effect is important.

We have given an expression for the spin echo signal in terms of diffusion modes. We have shown that the refocusing of the echo at time $t=2t_e$ originates in the symmetry of the linear field profile with respect with the center of the sample. In the presence of the spin rotation effect, the echo signal acquires a phase shift due to the reversal of the molecular field μM_0 following the 180° pulse. We have given explicit expressions for the echo amplitude and phase in the three limiting cases. In the free diffusion regime, the echo decays as $\exp[-\frac{2}{3}(\gamma G)^2 D_\perp t_e^3/(1+\mu^2 M_0^2)]$ in agreement with the expression given by Leggett.[2] In the motional narrowing regime, the echo decays exponentially according to the classical decay rate $\propto L^4(\gamma G)^2/D_\perp$. In the localization regime, decay of the echo is also exponential, with a decay rate $\propto(\gamma G)^{2/3}D_\perp^{1/3}(1+\mu^2M_0^2)^{-1/6}$.

Finally, the numerical calculations with realistic parameters show that the deviations from the free diffusion regime are not negligible. This stands as a warning to experimentalists since the deviations mimic the saturation of the transverse relaxation time at low temperature. We hope that our results will go some way to solving the current controversy on the spin diffusion anisotropy in degenerate Fermi liquids.

ACKNOWLEDGMENTS

The authors want to thank D. Candela, G. Vermeulen, and G. Eska for enlightening discussions. This work was supported by the EPSRC of Great Britain.

APPENDIX: NUMERICAL TECHNIQUES

We used two different methods to produce the results described in this article. The first method, based on matrix diagonalization, allows the calculation of diffusion modes and, hence all quantities of interest (NMR spectrum, overlap matrix, echo signal) using formulas (2) and (12). This method turns out to be limited by the computer precision for large $|b|$ and small $|\mu M_0|$. To overcome this problem, we have used an operator-based method, which we describe in the last part of this appendix.

1. Matrix method

A standard method of solving eigenvalue problems of the Schrödinger type is to use a representation in terms of eigenfunctions of the Laplace operator obeying the boundary conditions (see for example Candela *et al.*[7]). For a cylinder this orthonormal set of functions ψ_{nlm} is

$$\psi_{nlm}(\zeta,\rho,\varphi)=\Theta_n\Xi_{lm}\cos\left(\frac{n\pi}{2}(\zeta+1)\right)J_m(\kappa_{lm}\rho)e^{im\varphi},$$

where $0\leqslant\rho\leqslant1$ is the radial coordinate in expressed reduced units, φ is the azimuthal coordinate, J_m is the mth Bessel function, and κ_{lm} is the lth zero of the derivative of J_m. The normalization factors are given by

$$\Theta_0=1/\sqrt{2},\quad \Theta_n=1\quad n>0,$$

$$\Xi_{l0}=\frac{\sqrt{2}}{|J_0(\kappa_{l0})|},$$

$$\Xi_{lm}=\frac{\sqrt{2}}{|J_{m+1}(\kappa_{lm})|}\quad m>0.$$

In the case of a linear field profile we treat in this article, the problem is one dimensional, so we use the subset of functions ψ_{n00}, i.e., a Fourier expansion.

The ''Hamiltonian'' of the diffusion problem is $\hat{H}=\partial_\zeta^2+ib\zeta$. The matrix elements of the Hamiltonian in the cosine representation can be calculated analytically straightforwardly. Practically, of course, we calculate only a finite number of matrix elements. Since the number of relevant modes scales as $\propto L/L_c=b^{1/3}$, we used $N\times N$ matrices with $N>6b_1^{1/3}$ to avoid any aliasing effect. This matrix was then diagonalized using the software package MATLAB to obtain the eigenfrequencies and the Fourier components of the diffusion modes.

We note V, the square matrix whose columns are the eigenvectors of H. By contrast with quantum mechanics, the Hamiltonian is non-Hermitian, so its eigenvalues are complex and the matrix V is not unitary. However, H is symmetric so the matrix V is orthogonal:

$$V^t\cdot V=I, \tag{A1}$$

V^t being the transpose of the matrix V (*not* the Hermitian adjoint) and I the identity matrix. If the initial magnetization is uniform, the vector of the weights of the modes in the free induction decay [Eq. (2)] is the first row of the matrix V (i.e., $c_n=V_{0n}$).

To calculate the spin echo signal, we need to consider the two Hamiltonians $\hat{H}_<=\partial_\zeta^2+ib\zeta$ and $\hat{H}_>=\partial_\zeta^2+ib^*\zeta$. We note $V_>$ and $V_<$, the matrices of eigenvectors of, respectively, $H_>$ and $H_<$. The overlap matrix is given by

$$U=V_>^\dagger\cdot V_<, \tag{A2}$$

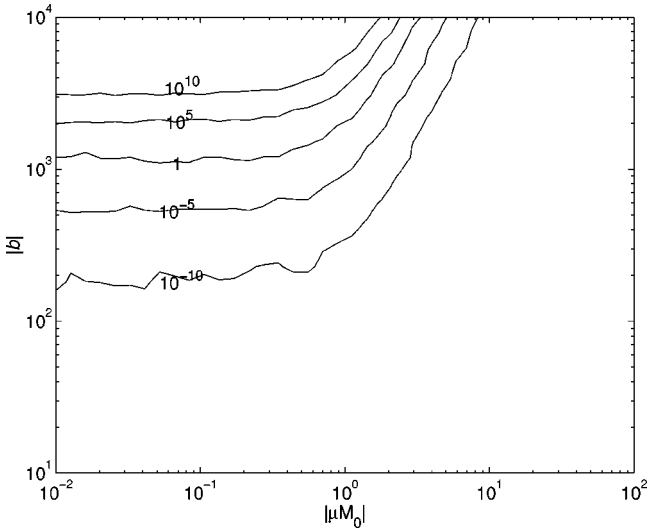

FIG. 8. Contour line map of the norm of the matrix $(V\cdot {}^tV-I)$ calculated with 100×100 elements. In this example, the region of parameters where the method fails is $|b|\gtrsim 500$ and $|\mu M_0|\lesssim 2$.

where † denotes the Hermitian adjoint. From Eq. (A2), it is easy to see that U is also an orthogonal matrix, since $V_>$ and $V_<$ are orthogonal matrices. In the case of a linear field profile, the expression for U can be simplified further:

$$U=I-2V_{even}^{t}\cdot V_{even}, \tag{A3}$$

where V_{even} is the $N\times N/2$ matrix whose columns are the even columns of $V_>$, so only one set of modes needs to be calculated. From the matrices U,V and the eigenvalues, the echo signal is calculated using formula (12).

2. Accuracy of the matrix method

Numerically, the matrix method fails when $|b|$ is large and $|\mu M_0|$ is small. In such a case, the elements of the matrix V take very large values. This is not a problem for calculating the FID signal, since the weighting coefficients c_n are always determined with sufficient accuracy. However, the small errors in the elements of the matrix V build up when one calculates the matrix product $V_{even}^{t}\cdot V_{even}$. This results in large errors in the overlap matrix U and thus prevents us from computing the amplitude of the echo signals accurately.

An indication that the computer accuracy is not sufficient is that the orthogonality relation (A1) is violated numerically. In Fig. 8, we show a contour line map of the norm of the matrix $(V\cdot {}^tV-I)$ calculated with 100×100 elements (the norm being defined as the largest column sum). The region where this norm is $>10^{-5}$ (say) corresponds to the range of parameters where the orthogonality relation (A1) is numerically not obeyed. In the example shown the region of parameters where the method fails is $|b|\gtrsim 500$ and $|\mu M_0|\lesssim 2$. The accuracy of the method can be enhanced by using larger matrices, but at a large cost in term of computation time. For example, the region of parameters where the method fail recedes to $|b|\gtrsim 1000$ and $|\mu M_0|\lesssim 1$ if we use 300×300 elements. Attempts to use alternative diagonalization methods failed to improve the accuracy of the matrix V. It is worth noting that, in the case of a quadratic field profile with a cylindrical geometry, this numerical problem does not occur for the radial eigenvalue problem.

3. Operator method

Although knowledge of the eigenmodes is useful for understanding the underlying physics of the diffusion problem, it is not necessary to calculate the FID signal or the echo signal. Using a method similar to that of Schneider and Freed,[18] we can obtain the magnetization evolution $|m_-(\tau)\rangle$ (here we use the usual Dirac's notations) by iterating the "Schrödinger equation" from the given initial condition $|m_-0)\rangle$:

$$|m_-(\tau+d\tau)\rangle=(1+\hat{H}d\tau)|m_-(\tau)\rangle. \tag{A4}$$

The time τ is now expressed in units of $L^2/D_{\rm eff}$ to make the formula dimensionally correct.

An alternative method consists in calculating $|m_-(\tau)\rangle$ directly by application of the evolution operator $e^{\hat{H}\tau}$:

$$|m_-(\tau)\rangle=e^{\hat{H}\tau}|m_-(0)\rangle. \tag{A5}$$

By writing out the ket $|m_-(0)\rangle$ as a linear combination of eigenvectors of $\hat{H}$, it is easy to show the equivalence between Eq. (A5) and Eqs. (2) and (3). From Eq. (A5), we calculate the NMR signal:

$$S(\tau)=\langle m_-(0)|e^{\hat{H}\tau}|m_-(0)\rangle. \tag{A6}$$

The calculation of the spin echo signal follows the same lines: the Hamiltonian $\hat{H}_<$ governs the magnetization during the evolution period. The π pulse at time τ_e changes $|m_-(\tau_e)\rangle$ into $-\langle m_-(\tau_e)|$ and b into b^*. After the π pulse, the evolution is determined by the Hamiltonian $\hat{H}_>$. So the equivalent of Eq. (12) for the echo signal is

$$\begin{aligned} S(\tau)&=-\langle m_-(\tau_e)|m_-(\tau-\tau_e)\rangle \\ &=-\langle m_-(0)|e^{\hat{H}_<^{\dagger}\tau_e^*}e^{\hat{H}_>(\tau-\tau_e)}|m_-(0)\rangle. \end{aligned} \tag{A7}$$

Formulas (A6) and (A7) do not lend themselves to analytical calculations. However, we can use the geometric interpretation of the kets as vectors in a Hilbert space to gain insight into the difference between the classical case and the quantum case. Let us consider the pure quantum case $(|\mu M_0|=+\infty)$ first. Similarly to quantum mechanics, the Hamiltonian is Hermitian, so the evolution operator is a rotation in Hilbert space. This implies that, during the magnetization evolution, the norm of the ket $|m_-(\tau)\rangle$ is constant:

$$\langle m_-(\tau)|m_-(\tau)\rangle=\langle m_-(0)|m_-(0)\rangle. \tag{A8}$$

This equality points to the fact that, in the pure quantum case, the signal decay is reversible and entirely due to decoherence by inhomogeneous broadening. Despite the reversible nature of the signal decay, the magnetization is not refocused completely by the Hahn echo, because the rotation undergone by $|m_-(0)\rangle$ during the evolution is not canceled

by the rotation undergone by $|m_-(\tau_e)\rangle$ between time τ_e and $2\tau_e$. Geometrically, $|m_-(\tau_e)\rangle$ and $|m_-(0)\rangle$ have the same norm, but lie at different angles in the Hilbert space.

In the pure classical case ($\mu M_0=0$), the norm of $|m_-(\tau)\rangle$ decreases with increasing τ because the evolution operator is not unitary. Physically, it means that both reversible inhomogeneous broadening and irreversible diffusion processes contribute to the signal decay. In the pure classical case, one has $\hat{H}_<=\hat{H}_>$, so the expression of the spin echo signal reduces to

$$|S(2\tau_e)|=\langle m_-(\tau_e)|m_-(\tau_e)\rangle\leqslant\langle m_-(0)|m_-(0)\rangle. \tag{A9}$$

Contrary to the pure quantum case, $|m_-(\tau_e)\rangle$ and $|m_-(0)\rangle$ lie at the same angle in the Hilbert space, but have different norms. The physical interpretation is that the Hahn echo completely refocuses the inhomogeneous broadening, and the echo attenuation is due to diffusion only.

We have used the cosine representation defined above to implement the iteration method and the evolution operator method. The iteration was carried out with a fourth-order Runge-Kutta routine, and the evolution matrix $e^{H\tau}$ was calculated using a numerical matrix exponential function, both provided by MATLAB. These two methods give accurate results for all values of the parameters b and μM_0. The iteration method was found faster than the evolution operator method, but care had to be taken when the iteration was carried out backwards, since the system is unstable for negative times. One of the reasons why the operator method is more accurate than the matrix diagonalization method is that no scalar product operation is actually required to calculate the FID or spin echo signals if the initial condition is $m_-(\zeta,0)=\langle\zeta m_-(0)\rangle=1$: thanks to the cosine representation, the vector of Fourier coefficients of the magnetization $m_-(\zeta,\tau)$ is the first column of the matrix $e^{H\tau}$, so the NMR signal and the echo signal are simply the upper left element of the matrices $e^{H\tau}$ and $e^{H_<^\dagger\tau_e^*}e^{H_>(\tau-\tau_e)}$, respectively.

[1] T.M. Swiet and P.N. Sen, J. Chem. Phys. **100**, 5597 (1994).
[2] A.J. Leggett, J. Phys. C **3**, 448 (1970).
[3] C. Lhuillier and F. Laloe, J. Phys. (Paris) **43**, 225 (1982).
[4] G. Vermeulen and A. Roni, Phys. Rev. Lett. **86**, 248 (2001); A. Roni and G.A. Vermeulen, Physica B **280**, 87 (2000).
[5] J.R. Owers-Bradley, R.M. Bowley, O. Buu, D. Clubb, and G.A. Vermeulen, J. Low Temp. Phys. **121**, 779 (2000).
[6] R.J. Ragan, J. Low Temp. Phys. **98**, 489 (1995).
[7] D. Candela, N. Masuhara, D.S. Sherrill, and D.O. Edwards, J. Low Temp. Phys. **63**, 369 (1986).
[8] S.D. Stoller, W. Happer, and F.J. Dyson, Phys. Rev. A **44**, 7459 (1991).
[9] J.H. Freed, Ann. Phys. (Paris) **10**, 901 (1985).
[10] *Handbook of Mathematical Functions*, edited by M. Abramowitz and I. A. Stegun (Dover, New York, 1965).
[11] E.L. Hahn, Phys. Rev. **80**, 580 (1950).
[12] B. Robertson, Phys. Rev. **151**, 273 (1966).
[13] A.E. Meyerovich and K.A. Musaelian, J. Low Temp. Phys. **94**, 249 (1994); **95**, 789 (1994); **72**, 1710 (1994); Phys. Rev. Lett. **72**, 1710 (1994).
[14] I.A. Fomin, JETP Lett. **65**, 749 (1997).
[15] J.H. Ager, A. Child, R. König, J.R. Owers-Bradley, and R.M. Bowley, J. Low Temp. Phys. **99**, 683 (1995).
[16] L-J. Wei, N. Kalechofsky, and D. Candela, Phys. Rev. Lett. **71**, 879 (1993).
[17] H. Ishimoto, H. Fukuyama, T. Fukuda, T. Tazaki, and S. Ogawa, Phys. Rev. B **38**, 6422 (1988).
[18] D.J. Schneider and J.H. Freed, Adv. Chem. Phys. **73**, 387 (1989).